Fast iterative algorithm for the reconstruction of multi-shot non-Cartesian diffusion data

Merry Mani[1]*, Mathews Jacob*[2]*, Vincent Magnotta*[3]*, Jianhui Zhong*[4]

[1]*Department of Electrical and Computer Engineering, University of Rochester, NewYork*

[2]*Department of Electrical and Computer Engineering, University of Iowa , Iowa*

[3]*Department of Radiology, University of Iowa, Iowa*

[4]*Department of Biomedical Engineering, University of Rochester, NewYork*

August 25, 2014

Correspondence to :

Jianhui Zhong

University of Rochester Medical Center, Box 648

601 Elmwood Avenue

Rochester, NY 14642-8648.

email: jzhong3@gmail.com

phone number: (585) 273-4518.

Word count : 2820

Figures+ tables count : 5

Running title: Fast iterative reconstruction algorithm for multi-shot non-Cartesian diffusion data

Abstract

Purpose:

To accelerate the motion-compensated iterative reconstruction of multi-shot non-Cartesian diffusion data.

Method:

The motion-compensated recovery of multi-shot non-Cartesian diffusion data is often performed using a modified iterative sensitivity encoded (SENSE) algorithm. Specifically, the encoding matrix is replaced with a combination of non-uniform Fourier transforms and composite sensitivity functions, which account for the motion-induced phase errors. The main challenge with this scheme is the significantly increased computational complexity, which is directly related to the total number of composite sensitivity functions (number of shots $\times$ number of coils). The dimensionality of the composite sensitivity functions and hence the number of Fourier transforms within each iteration is reduced by using a principal component analysis (PCA)-based scheme. Using a Toeplitz-based conjugate gradient approach in combination with an augmented Lagrangian optimization scheme, a fast algorithm is proposed for the sparse recovery of diffusion data.

Results:

The proposed simplifications considerably reduce the computation time, especially in the recovery of diffusion data from under-sampled reconstructions using sparse optimization. By choosing appropriate number of basis functions to approximate the composite sensitivities, faster reconstruction (close to 9 times) with effective motion compensation is achieved.

Conclusion:

The proposed enhancements can offer fast motion-compensated reconstruction of multi-shot diffusion data for arbitrary k-space trajectories.

Keywords: motion-compensated diffusion imaging, multi-shot diffusion imaging, Toeplitz-embedding,

principal component analysis, under-sampled reconstruction for high resolution diffusion imaging, augmented Lagrangian.

Introduction

The use of multi-shot non-Cartesian parallel MRI acquisitions is emerging as a popular scheme for high spatial resolution diffusion weighted imaging. Multi-channel acquisition provides improved signal-to-noise ratio (SNR), while the segmented k-space readouts reduce the echo train length which in turn reduces the T2* decay and geometric distortions caused by magnetic field inhomogeneities [1–5]. Combined with non-Cartesian acquisitions such as SNAILS [6], PROPELLER [7] etc., high spatial resolutions using matrix sizes of up to 512 x 512 were achieved in diffusion-weighted images (DWIs) with significantly diminished distortions [2]. However, a primary shortcoming of the above multi-shot method for diffusion weighted imaging is the sensitivity of the modality to motion-induced artifacts [8–11]. While rigid body motion resulting from subject motion can induce linear phase perturbations, physiologically induced motion such as blood and cerebrospinal fluid pulsation can cause nonlinear phase errors that will result in significant ghosting artifacts [1, 3]. Several algorithms have been proposed to account for motion artifacts in DWI. Linear phase errors resulting from rigid body motion result in shifts in k-space, which can be relatively easily corrected in k-space and can be de-coupled from the image reconstruction [12, 13]. However, non-linear phase errors cannot be corrected this way. The approach typically followed is to subtract an estimate of the phase errors from each shot. The phase errors are estimated either from an additional navigator scan or from the fully sampled center of a self-calibrating k-space trajectory and computing a low-resolution phase map from the navigator region of each shot [5, 6, 14]. It has been shown that correction of non-linear phase errors can be reformulated as an iterative SENSE reconstruction scheme and it works better than a simple phase subtraction [2, 15].

While iterative reconstruction methods can offer excellent motion-compensation, these methods are inherently slow, especially when multi-dimensional datasets are involved. Since phase errors are different for each coil and each shot, the number of sensitivity functions to be accommodated in the iterative SENSE reconstruction is often large. Also, because the number of Fourier transforms at each iteration scales with the number of sensitivity functions, the computational complexity increases considerably with the number of shots and coils. Our own motivation in the problem is in the context of motion-compensated reconstruction of high spatial and angular resolution (typically > 60 DWIs) diffusion data. To reduce the acquisition time, these measurements are highly under-sampled; the recovery is performed using non-linear reconstruction schemes such as compressed sensing (CS) [16–18] to reconstruct the multi-directional diffusion data [19–21].

We aim to accelerate the reconstruction algorithm by exploiting the redundancy and smoothness of the

phase maps using dimensionality reduction techniques. Specifically, we compress the phase maps corresponding to each shot and each coil using a principal component analysis (PCA). Note that this method is different from the PCA-based coil compression methods [22, 23], which reduce the dimensionality of the k-space data itself before performing the image reconstruction; these schemes are infeasible in our setting since the k-space trajectory for each composite sensitivity is different. In contrast, we propose a synthesis formulation (see Figure 1 in supporting information) wherein we represent the composite sensitivity functions of all the channels using a single PCA basis set. This enables us to exploit the redundancy of the composite sensitivity functions along the channels as well as shots, thus enabling higher accelerations than what is offered by the convention channel compression schemes. We show that the proposed simplified scheme can enable fast joint reconstruction of the multi-dimensional data without compromising the quality of motion-compensation. In the following sections, we first describe the simplified motion-compensation approach and then extend it to accelerated recovery from under-sampled acquisitions.

Methods

Liu et al., have formulated the forward model that describes the diffusion encoded k-space acquisition for the $\mathbf{q^{th}}$ diffusion direction as [2]:

$$m_c(\mathbf{k}_{q,i}) = \sum_{\mathbf{r}} s_q(\mathbf{r})\, p_{c,q,i}(\mathbf{r})\, e^{-j2\pi \mathbf{k}_{q,i}^{\mathbf{T}}\mathbf{r}}, \tag{1}$$

where m_c is the k-space measurement at the k-space location $\mathbf{k}$ on the i^{th} shot using coil c. Here, $s_q(\mathbf{r})$ is the diffusion signal at voxel location $\mathbf{r}$ for the q^{th} diffusion weighted image, $p_{c,q,i}(\mathbf{r})$ is the motion induced phase error, which is also weighted by the coil sensitivities (also referred to as composite sensitivities), for the voxel location $\mathbf{r}$ for the c^{th} coil, i^{th} shot and q^{th} diffusion direction. $e^{-j2\pi \mathbf{k}_{q,i}^{\mathbf{T}}\mathbf{r}}$ are the Fourier exponentials for the arbitrary k-space locations. For a given diffusion direction, the system of measurements in Eq. (1) in matrix form is given by:

$$\mathbf{m} = \mathbf{E}\mathbf{s} + \epsilon, \tag{2}$$

where $\mathbf{m}$ is the vector of k-space measurements of size $(N_{\mathrm{k}} \times N_{\mathrm{i}} \times N_{\mathrm{c}}) \times 1$; N_{k}, N_{i}, and N_{c} are respectively the number of k-space points per shot, the number of shots, and the number of channels. The matrix of Fourier exponentials combined with the composite sensitivities form the encoding function $\mathbf{E}$ and ϵ is the Gaussian-distributed measurement noise in k-space. The reconstruction of the vectorized image $\mathbf{s}$ is then

solved as an iterative SENSE recovery problem [24], often solved using conjugate gradients (CG):

$$\mathbf{s}^* = \arg\min_{\mathbf{s}} \|\mathbf{E}\mathbf{s} - \mathbf{m}\|_{\ell_2}^2. \tag{3}$$

The flowchart showing the update of $\mathbf{s}$ using the CG-SENSE algorithm is given in Figure 1(a). At each iteration, we need to compute $\mathbf{h} = \mathbf{E}^H\mathbf{E}\mathbf{s}$, where $\mathbf{E}^H$ represents the adjoint of $\mathbf{E}$.

$$\mathbf{E}^H\mathbf{E} = \sum_{l=1}^{N_i \times N_c} \left(\mathbf{P}_l^H\, \mathbf{Q}_l^H\, \mathbf{Q}_l\, \mathbf{P}_l\right). \tag{4}$$

Here, $\mathbf{Q}_l$ is the non-uniform discrete Fourier transform that maps the image to the k-space samples corresponding to the l^{th} shot. $\mathbf{P}_l = \mathrm{diag}(p_l(\mathbf{r}))$ is a diagonal matrix, whose diagonal entries correspond to the l^{th} composite sensitivity function $p_l(\mathbf{r})$. Note that the computation of the above equation requires $N_c \times N_i$ non-Cartesian Fourier transforms and inverse transforms, per iteration (see Figure 1(a)); the computational complexity of this step is the key bottleneck in achieving fast implementation. We use a three step strategy to considerably reduce the computation time. The main components are described in the following sections.

Step 1: Dimensionality Reduction using PCA

The number of non-uniform Fourier transforms to be evaluated at each iteration is equal to the number of composite sensitivity functions ($M = N_i \times N_c$ per diffusion direction). We now propose to reduce the number of non-uniform Fourier transforms by exploiting the redundancy in the composite sensitivity functions. The central idea is to approximate the composite sensitivity functions $p_l(\mathbf{r}); l = 1, .., M$ as a linear combination of N_b basis functions, $c_j(\mathbf{r}); j = 1, .., N_b$:

$$p_l(\mathbf{r}) \approx \sum_{j=1}^{N_b} a_{l,j}\, c_j(\mathbf{r});\;\; l = 1, .., M \tag{5}$$

where $a_{l,j}$ are the scalar coefficients. Since each composite sensitivity function is a linear combination of the same N_b basis functions, the number of non-uniform Fourier transforms required to evaluate $\mathbf{E}^H\mathbf{E}$ reduces from M to $N_b; N_b << M$.

We use a principal component analysis to determine the optimal basis functions for representing the composite sensitivity functions. We stack the vectorized composite sensitivity functions into the columns of a matrix $\mathbf{Z}$ and perform a singular value decomposition, $\mathbf{Z} = \mathbf{U}\mathbf{\Sigma}\mathbf{\Lambda}^H$. The left singular vectors, $\mathbf{U}$, correspond to the basis functions, while $\mathbf{\Sigma}\mathbf{\Lambda}^H$ are the coefficients. One can choose the number of basis functions,

N_b, so as to obtain the desired approximation quality; a good guess can be obtained by plotting the singular values of $\mathbf{\Sigma}$. Note that this approach is different from the conventional PCA-based channel compression schemes where the k-space data is compressed (see Figure 1 supporting information). Other choices of basis functions such as polynomials can also be used [25] (see section 1.1 in supporting information).

Step 2 : Integrate PCA-based approximation and Toeplitz embedding

The evaluation of forward and backward non-uniform Fourier transforms within each iteration is computationally expensive. To speed up this computation, the Toeplitz structure of $\mathbf{Q}_l^H\mathbf{Q}_l$ can be exploited [26–29]. This enables to rewrite $\mathbf{Q}_l^H\mathbf{Q}_l = \mathbf{F}^H\ \mathbf{W}_l\ \mathbf{F}$, where the $(2N)^2 \times (2N)^2$ matrix $\mathbf{F}$ corresponds to the uniform discrete Fourier transform that maps the $N \times N$ image to the $2N \times 2N$ grid in the Fourier domain. Note that $\mathbf{F}$ can be efficiently implemented using zero-padded fast Fourier transform. $\mathbf{W}_l$ is a $(2N)^2 \times (2N)^2$ diagonal matrix whose diagonal entries correspond to the $2N \times 2N$ DFT of $w_l(\mathbf{r}) = \sum_{\mathbf{k}_l} e^{-j2\pi\mathbf{k}_l^{\mathrm{T}}\mathbf{r}}$; k_l denotes the k-space location of the shot corresponding to l.

Combining step 1 and 2 described above, Eq. (4) can be simplified as:

$$\mathbf{h} = \mathbf{E}^H\mathbf{E}\mathbf{s} = \sum_{l=1}^{M} \left(\mathbf{P}_l^H\ \mathbf{F}^H\ \mathbf{W}_l\ \mathbf{F}\ \mathbf{P}_l\right)\ \ \mathbf{s}, \tag{6}$$

replacing the non-uniform Fourier transforms by fast Fourier transforms. Since the Fourier transforms are linear, we can simplify the Fourier transform of the sensitivity weighed image as $\mathbf{F}\,\mathbf{P}_l\,\mathbf{s} = \sum_{j=1}^{N_b} a_{l,j}\,(\ \mathbf{F}\,\mathbf{C}_j\ \mathbf{s})$. Here, $\mathbf{C}_j$ is a diagonal matrix, whose diagonal entries correspond to the j^{th} basis function $c_j(\mathbf{r})$. Further simplification of $\mathbf{E}^H\mathbf{E}$ follows:

$$\begin{aligned}
\mathbf{E}^H\mathbf{E} &= \sum_{l=1}^{M} \underbrace{\sum_{k=1}^{N_b} a_{l,k}^{*}\left(\mathbf{C}_k^H\,\mathbf{F}^H\right)}_{\mathbf{P}_l^H\mathbf{F}^H}\ \mathbf{W}_l\ \underbrace{\sum_{j=1}^{N_b} a_{l,j}\mathbf{F}\mathbf{C}_j}_{\mathbf{F}\mathbf{P}_l} \\
&= \sum_{l=1}^{M}\sum_{k=1}^{N_b}\sum_{j=1}^{N_b} a_{l,j}\ a_{l,k}^{*}\left(\mathbf{C}_k^H\mathbf{F}^H\mathbf{W}_l\mathbf{F}\mathbf{C}_j\right) \\
&= \sum_{k=1}^{N_b}\sum_{j=1}^{N_b} \mathbf{C}_k^H\mathbf{F}^H \underbrace{\left(\sum_{l=1}^{M} a_{l,j}a_{l,k}^{*}\mathbf{W}_l\right)}_{\mathbf{U}_{j,k}} \mathbf{F}\mathbf{C}_j
\end{aligned} \tag{7}$$

The simplification of $\mathbf{E}^H\mathbf{E}$ using Eq. (7) is graphically illustrated in Figure 1(d). While Toeplitz-embedding is standard in non-Cartesian MRI reconstruction, the combination of the weights corresponding to the different trajectories specified by $\mathbf{U}_{jk}$ introduced above is a novel formulation. Since the composite

sensitivity functions are smooth and have significant redundancy between them, the above approximation is often very good for even small values of N_b. Note that the computation of the above expression requires only N_b FFT and IFFT operations, instead of $M >> N_b$, resulting in faster computations and reduced memory demands.

Step 3: Image recovery from under-sampled data using augmented Lagrangian algorithm

The above simplification will considerably accelerate the CG-SENSE recovery of fully-sampled [30] or moderately under-sampled reconstructions. As described earlier, our own motivation is to use this scheme for under-sampled reconstructions using CS-based schemes; these methods use additional regularization priors to exploit the structure imposed by various sparse diffusion models [19, 20, 31]. Existing formulations of such schemes has a general form:

$$\mathbf{x}^* = \arg\min_{\mathbf{x}} \mathcal{C}(\mathbf{x}) \text{ where } \quad \mathcal{C}(\mathbf{x}) = ||\mathbf{A}\mathbf{x} - \mathbf{y}||_{\ell_2}^2 + \lambda_{\mathbf{1}}||\mathbf{B}\mathbf{x}||_{TV} + \lambda_{\mathbf{2}}||\mathbf{G}\mathbf{x}||_{\ell_1}, \tag{8}$$

where some formulations use both TV and ℓ_1 constraints [19, 20, 31], while others use only the ℓ_1 constraint [32]. Here, $\mathbf{y}$ is the under-sampled k-space measurements for all diffusion directions, $\mathbf{A}$ is the consolidated forward model, $||\mathbf{B}\mathbf{x}||_{TV}$ is the total-variation (TV) norm of the unknown vector $\mathbf{x}$ in some transform domain $\mathbf{B}\mathbf{x}$, $||\mathbf{G}\mathbf{x}||_{\ell_1}$ is the ℓ_1 norm of $\mathbf{x}$ in some transform domain $\mathbf{G}\mathbf{x}$, $\lambda_{\mathbf{1}}$ and $\lambda_{\mathbf{2}}$ are regularization parameters controlling the weights. The TV norm is defined as $||\mathbf{x}||_{TV} = ||\sqrt{\sum_{k=1}^{2} |\mathbf{R_k}\mathbf{x}|^2}||_{\ell 1}$ where $\mathbf{R_1}$ and $\mathbf{R_2}$ are the finite difference matrices along the x- and y- dimensions, and the ℓ_1 norm is defined as $||\mathbf{x}||_{\ell_1} = \sum |\mathbf{x}_i|$.

Due to the compound nature of the regularizations, problems of the form in Eq. (8) are typically solved using variable splitting techniques such as the classical augmented Lagrangian (AL) approach [33, 34] or the split Bregman approach [20]. These techniques convert the above unconstrained problem to a constrained form through introduction of auxiliary variables:

$$\mathcal{C}_1(\mathbf{x}) = \|\mathbf{A}\mathbf{x} - \mathbf{y}\|_{\ell_2}^2 + \lambda_{\mathbf{1}}\sqrt{\sum_{k=1}^{2} |\mathbf{g_k}|^2} + \lambda_{\mathbf{2}}||\mathbf{y}||_{\ell_1} \text{ such that } \mathbf{y} = \mathbf{G}\mathbf{x} \text{ and } \mathbf{g_k} = \mathbf{R_k}\mathbf{B}\mathbf{x}. \tag{9}$$

Here, $\mathbf{y}$ and $\mathbf{g}$ are the auxiliary variables. The constrained form of Eq. (9) is easier to solve. The AL algorithm for optimizing the cost function in Eq. (9) is included below. The algorithm alternates between

the quadratic subproblem

$$\mathbf{x}^{n+1} = \arg\min_{\mathbf{x}} ||\mathbf{A}\mathbf{x} - \mathbf{y}||_{\ell_2}^2 + \frac{\beta_1}{2}\sum_{k=1}^{2} ||\mathbf{g_k} - \mathbf{R_k}\mathbf{B}\mathbf{x}||^2 - \sum_{k=1}^{2} {\gamma_{1_k}}^T(\mathbf{g_k} - \mathbf{R_k}\mathbf{B}\mathbf{x}) + \frac{\beta_2}{2}||\mathbf{y} - \mathbf{x}||^2 - {\gamma_\mathbf{2}}^T(\mathbf{y} - \mathbf{x}), \quad (10)$$

and simpler shrinkage steps given in Eq. (11-13). Of these updates, the computationally expensive step is the one in Eq. (10), which is solved using CG. Here, we propose to express $\mathbf{A}^H\mathbf{A}$ in terms of $\mathbf{E}_q^H\mathbf{E}_q; q = 1, .., N_q$, for the recovery of the q^{th} diffusion direction, each of which can be efficiently computed as described in the previous subsection.

Algorithm Augmented Lagrangian algorithm for minimizing the cost in Eq. (8)

1: Initialize $x^{(0)}$, $y^{(0)}$, ${g_k}^{(0)}$, $\beta_1 > 0$, $\beta_2 > 0$,γ_{1k},γ_2
2: set $n = 0$
3: Repeat
4: $x^{(n+1)}$: Solve Eq. (10) using CG.
5: $y^{(n+1)}$: Update using the ℓ_1 shrinkage rule:[35]

$$\mathbf{y}^* = \text{sign}(\mathbf{x} + \frac{\gamma_\mathbf{2}}{\beta_2})\big(|\mathbf{x} + \frac{\gamma_\mathbf{2}}{\beta_2}| - \frac{1}{\beta_2}\big)_+. \quad (11)$$

6: $g_k^{(n+1)}$: Update using the multi-dimensional TV shrinkage rule : [35–37]

$${\mathbf{g_k}}^* = \frac{\mathbf{R_k}\mathbf{x} + \frac{\gamma_\mathbf{k}}{\beta_1}}{\sqrt{\sum_{k=0}^{1}|\mathbf{R_k}\mathbf{x} + \frac{\gamma_\mathbf{k}}{\beta_1}|^2}}\left(\sqrt{\sum_{k=0}^{1}|\mathbf{R_k}\mathbf{x} + \frac{\gamma_\mathbf{k}}{\beta_1}|^2} - \frac{1}{\beta_1}\right)_+. \quad (12)$$

7: Update Lagrange multipliers:

$$\begin{aligned} {\gamma_\mathbf{2}}^{n+1} &= \gamma_\mathbf{2} - \beta_2(\mathbf{y} - \mathbf{x}) \\ {\gamma_{\mathbf{1_k}}}^{n+1} &= \gamma_{\mathbf{1_k}} - \beta_1(\mathbf{g_k} - \mathbf{R_k}\mathbf{x}). \end{aligned} \quad (13)$$

8: set $n = n + 1$
9: Until stopping criterion is reached

Datasets for Validation

In-vivo datasets from two healthy adult volunteers were used for validation. The datasets were collected in accordance with the Institutional Review Board of the University of Iowa on a Siemens 3T MR scanner with maximum gradient amplitude of 45 mT/m and slew rate of 200 T/m/sec using a 12 channel head coil. 64 DWIs (b-value =1200 s/mm^2) and one non-diffusion weighted image were collected using a SNAILS

sequence with the following specifications: FOV = 20cm, matrix size = 192x192, TE/TR $= 61/2500$ms. Dataset1 was collected using a fully sampled acquisition, prescribed as follows: 10 slices were acquired with slice-thickness of 2.5mm using 22 spatial shots, variable density factor $(\alpha) = 8$, readout duration = 18.6ms, total scan time= 60mins. This dataset was retrospectively under-sampled to achieve a reduction factor (R) of 8 (keeping only 3 out of 22 spatial shots) giving an equivalent scan time of 8 mins. Dataset2 was prospectively collected at R=8. 38 slices were acquired with slice-thickness of 1.5mm, total scan time = 28mins. In all instances, the non-diffusion weighted images are fully sampled and the incoherent k-q scheme reported in Mani et al. [19] was used to under-sample the DWIs.

Results

We focus on reconstructing the 64 DWIs jointly employing the CS reconstruction given in Eq. (8) using the algorithm given above. All computations were performed using MATLAB on a 4-core Linux workstation with a 3.6GHz Intel Xeon processor with 32GB RAM. Under-sampled measurements at R=8 were used. The coil sensitivities were computed using the sum-of-squares method from the non-diffusion weighted images. The DWIs were first jointly reconstructed using a regular CG-SENSE reconstruction without accounting for motion-induced phase errors. As expected, significant signal drop-outs are observed in the reconstructed images. Representative images from three diffusion weightings are shown in Figure 2; Figure 2a correspond to the motion-uncompensated reconstruction using dataset1.

With composite sensitivities estimated from the over-sampled center-k-space of each shots corresponding to every diffusion direction, the images were reconstructed with motion compensation using the traditional implementation of $\mathbf{E^H E s}$ shown in Figure 1a. As can be observed from Figure 2b, the resulting images are free of motion artifacts. However, the time to reconstruct the artifact-free DWIs was about 13.6 hours using the above method, with about 37 sec spent per computation of $\mathbf{E^H E s}$. The reconstruction time using this method scales linearly with the number of composite sensitivities (M) per DWI. Note that M increases with the number of shots and the number of channels. To appreciate the computational complexity and memory demands of the traditional implementation, we tabulate in Table 1 the scaling of these parameters with M.

Next, the same motion-compensated reconstruction was implemented using the proposed simplification shown in Figure 1d. For the first experiment, N_b was chosen to be the same as M (=36) for the case of R=8 so that there is no approximation. Results of this implementation are shown in Figure 2c; note that even without reducing the dimensionality, the reconstruction was $1.33\times$ faster (time=10.22 hours) compared to

the traditional implementation. In the subsequent experiments, N_b was varied to take values of 18, 10 and 5 and the reconstruction was repeated. In Figure 3a, we plot the time spent per computation of $\mathbf{E^H E s}$ as well as the memory demands for N_b=5, 10, 18 and 36. The reconstruction time and the memory requirements scales with the number of basis functions. Figure 2d show the results for the reconstruction with N_b=5. The time of reconstruction was 1.45 hours, about 9$\times$ faster compared to the traditional implementation. To quantify the errors in the reconstructions, in Figure 3b, we report the normalized sum-of-squares error of the reconstructed images as a function of the number of basis functions used. As observed from Figures 2 and 3b, the loss in image quality while using as low as 5 basis functions is minimal compared to using all the basis functions. In all cases, λ_1 and λ_2 were empirically chosen to give the best visual results.

The DWIs were collected at high angular and spatial resolution so that they can be later used to reconstruct fiber orientations in each voxel. To further verify that these high resolution fiber orientation information were not lost during the reconstruction when using different number of basis functions, we computed the orientation distribution functions (ODF) [38] at a high angular resolution of 724 uniformly spaced directions and report the average angular error of the ODF and the success rate [39] in finding the correct number of diffusion components (see Figure 3c-d). Compared to the full PCA-bases, the average angular error was less than 2° and 3° and the success rate was close to 98 % and 97% for dataset1 and dataset2 respectively, verifying the quality of those reconstructions. The recovered high-resolution diffusion data were used for fiber tracking using the fiber-tracking module of the DSI studio software [40]. We compare the fiber tracking results from the same region of interest for the DWI reconstructed using N_b=36, 18, 10 and 5. Results in Figure 2 of supporting information show good agreement between the fiber tracking results, confirming the utility of the proposed approach.

Comparison with conventional channel compression

To demonstrate the performance difference between a conventional software channel compression (SCC) scheme [23] and the proposed scheme, we focus on recovering the motion-compensated DWI corresponding to a particular diffusion direction from fully-sampled data (12-channel, 22-shot) using the CG-SENSE reconstruction in Eq. (3). The k-space data is compressed to N_{scc} channels, followed by estimation of coils sensitivities and composite sensitivities from the compressed data for the purpose of motion-compensation. Figure 4 shows the comparison of the reconstruction quality as well as the reconstruction time using SCC, PCA-based and traditional CS-SENSE implementations. When the coils are compressed to a single virtual channel to achieve the least computation time, there is considerable loss in image quality.

Discussion and Conclusion

The above results show that the PCA-based approximation is capable of accounting for the motion-induced phase errors accurately, while enabling fast reconstruction of multi-dimensional datasets from under-sampled k-space measurements. It is also shown here that the large number of composite sensitivity functions can be compactly represented using a few number of principal components; around 5-10 principal components give very good approximation. With approximation using 5 basis functions, the reconstruction was 9 times faster, with minimal loss in accuracy. The number of basis functions can be chosen appropriately to achieve the desired accuracy. Further speed up can be obtained using GPU-based implementations. Our preliminary studies show speed up by a factor of 4-6 while using GPU-based implementations (23 mins for N_b=5; 98 mins for N_b=36). Computations based on over-lapping k-space blocks [41] can be used to further reduce memory demands while performing GPU-based computations. In addition, a matrix-formulation of $\mathbf{E}^H\mathbf{E}$ might enable to exploit the recently proposed matrix-inversion approach [42] to achieve even faster reconstructions. In conclusion, we have proposed a faster implementation for achieving motion-compensated CS reconstruction for multi-shot imaging for arbitrary k-space trajectories, which enables the reconstruction of high angular and spatial resolution DWI in a reasonable time.

List of figure captions

Figure 1: Various implementation of $\mathbf{E^H E s}$ (a) The traditional implementation of $\mathbf{E^H E s}$ in the update of $\mathbf{s}$ is shown. (b) and (c) are the intermediate steps that leads to the final simplified implementation in (d). The various symbols are defined as follows: $\mathbf{S_q}$ is the diffusion weighted image corresponding to the q^{th} diffusion direction, $\mathbf{P}_{q,i,j}$ are the composite sensitivity matrices corresponding to the q^{th} diffusion direction, i^{th} interleaf and j^{th} coil, $\mathbf{g}$ represents the gridding of Cartesian points to non-Cartesian grid followed by gridding back to Cartesian grid and $\mathbf{C}_j$ are the basis functions.

Figure 2: Diffusion weighted images reconstructed using various methods. (a) Images reconstructed using CG-SENSE without motion compensation, (b) motion-compensated reconstruction using traditional implementation of CG-SENSE, (c) & (d) are motion-compensated reconstruction using the proposed simplified implementation of CG-SENSE with 36 basis functions and 5 basis functions respectively. (e) and (f) are difference images (scaled to 1/12 the intensity of images in (b),(c),(d). The time (t) for the joint reconstruction of all DWIs are reported.

Figure 3: The scaling of different parameters with number of basis functions. (a) Memory demands and computation time per iteration of $\mathbf{E^H E s}$, (b) NSSE error for different number of basis functions, (c) Average ODF angular error for different number of basis functions, and (d) Success rate in finding the correct number of fiber orientations in a voxel for different number of basis functions.

Figure 4: Performance comparison between the proposed PCA-based method and the conventional channel compression (SCC). The reference image in (a) is obtained using the traditional implementation of CG-SENSE. The time to reconstruct a single diffusion direction is reported. (Difference images scaled to 1/4$^{\text{th}}$ of the dynamic range of reconstructed images.)

References

1 Holdsworth S. J, Skare S, Newbould R. D, and Bammer R. Robust GRAPPA-accelerated diffusion-weighted readout-segmented (RS)-EPI. Magn. Reson. Med., 2009, 62(6):1629–40.

2 Liu C, Moseley M. E, and Bammer R. Simultaneous phase correction and SENSE reconstruction for navigated multi-shot DWI with non-cartesian k-space sampling. Magn. Reson. Med., 2005, 54(6):1412–22.

3 Karampinos D. C, Van A. T, Olivero W. C, Georgiadis J. G, and Sutton B. P. High-resolution diffusion tensor imaging of the human pons with a reduced field-of-view, multishot, variable-density, spiral acquisition at 3 T. Magn. Reson. Med., 2009, 62(4):1007–16.

4 Uecker M, Karaus A, and Frahm J. Inverse reconstruction method for segmented multishot diffusion-weighted MRI with multiple coils. Magn. Reson. Med., 2009, 62(5):1342–8.

5 Nunes R. G, Jezzard P, Behrens T. E. J, and Clare S. Self-navigated multishot echo-planar pulse sequence for high-resolution diffusion-weighted imaging. Magn. Reson. Med., 2005, 53(6):1474–8.

6 Liu C, Bammer R, Kim D.-H, and Moseley M. E. Self-navigated interleaved spiral (SNAILS): application to high-resolution diffusion tensor imaging. Magn. Reson. Med., 2004, 52(6):1388–96.

7 Abe O, Mori H, Aoki S, Kunimatsu A, Hayashi N, Masumoto T, Yamada H, Masutani Y, Kabasawa H, and Ohtomo K. Periodically rotated overlapping parallel lines with enhanced reconstruction-based diffusion tensor imaging. Comparison with echo planar imaging-based diffusion tensor imaging. J. Comput. Assist. Tomogr., 2004, 28(5):654–60.

8 Trouard T. P, Sabharwal Y, Altbach M. I, and Gmitro A. F. Analysis and comparison of motion-correction techniques in diffusion-weighted imaging. J. Magn. Reson. Imaging, 1996, 6(6):925–35.

9 Chenevert T. L and Pipe J. G. Effect of bulk tissue motion on quantitative perfusion and diffusion magnetic resonance imaging. Magn. Reson. Med., 1991, 19(2):261–5.

10 Merboldt K. D, Hänicke W, Gyngell M. L, Frahm J, and Bruhn H. The influence of flow and motion in MRI of diffusion using a modified CE-FAST sequence. Magn. Reson. Med., 1989, 12(2):198–208.

11 Anderson A. W and Gore J. C. Analysis and correction of motion artifacts in diffusion weighted imaging. Magn. Reson. Med., 1994, 32(3):379–87.

12 Van A. T, Karampinos D. C, Georgiadis J. G, and Sutton B. P. K-space and image-space combination for motion-induced phase-error correction in self-navigated multicoil multishot DWI. IEEE Trans. Med. Imaging., 2009, 28(11):1770–80.

13 Wowk B, McIntyre M. C, and Saunders J. K. k-Space detection and correction of physiological artifacts in fMRI. Magn. Reson. Med., 1997, 38(6):1029–34.

14 Pipe J. G, Farthing V. G, and Forbes K. P. Multishot diffusion-weighted FSE using PROPELLER MRI. Magn. Reson. Med., 2002, 47(1):42–52.

15 Truong T.-K and Guidon A. High-resolution multishot spiral diffusion tensor imaging with inherent correction of motion-induced phase errors. Magn. Reson. Med., 2013. doi: 10.1002/mrm.24709.

16 Candes E, Romberg J, and Tao T. Robust Uncertainty Principles: Exact Signal Reconstruction from Highly Incomplete Frequency Information. IEEE Trans. Inf. Theory, 2006, 52(2):489–509.

17 Donoho D. Compressed sensing. IEEE Trans. Inf. Theory, 2006, 52(4):1289–1306.

18 Lustig M, Donoho D, Santos J, and Pauly J. Compressed Sensing MRI. IEEE Signal Process. Mag., 2008, 25(2): 72–82.

19 Mani M, Jacob M, Guidon A, Magnotta V, and Zhong J. Acceleration of high angular and spatial resolution diffusion imaging using compressed sensing with multichannel spiral data. Magn. Reson. Med., 2014. doi: 10.1002/mrm.25119.

20 Michailovich O, Rathi Y, and Dolui S. Spatially regularized compressed sensing for high angular resolution diffusion imaging. IEEE Trans. Med. Imaging., 2011, 30(5):1100–15.

21 Landman B. A, Wan H, Bogovic J. A, Bazin P.-L, and Prince J. L. Resolution of Crossing Fibers with Constrained Compressed Sensing using Traditional Diffusion Tensor MRI. In Proc. of SPIE, 7623, 2010; p. 76231H, number 8.

22 Buehrer M, Pruessmann K. P, Boesiger P, and Kozerke S. Array compression for MRI with large coil arrays. Magn. Reson. Med., 2007, 57(6):1131–9.

23 Huang F, Vijayakumar S, Li Y, Hertel S, and Duensing G. R. A software channel compression technique for faster reconstruction with many channels. Magn. Reson. Imag., 2008, 26(1):133–41.

24 Pruessmann K. P, Weiger M, Börnert P, and Boesiger P. Advances in sensitivity encoding with arbitrary k-space trajectories. Magn. Reson. Med., 2001, 46(4):638–51.

25 Sheng J, Ying L, and Liu B. Joint Estimation of Image and Coil Sensitivities in Parallel Spiral MRI. In IEEE Int. Symp. Biomed. Imaging (ISBI), 2007. IEEE. doi: 10.1109/ISBI.2007.356806.

26 Fessler J and Noll D. Iterative reconstruction methods for non-Cartesian MRI. In Proc. ISMRM Workshop on Non-Cartesian MRI. 2007.

27 Fessler J, Olafsson V, Shi H, and Noll D. Toeplitz-based iterative image reconstruction for MRI with correction for magnetic field inhomogeneity. IEEE Trans. Signal Process., 2005, 53(9):3393–3402.

28 Wajer F and Pruessmann K. Major Speedup of Reconstruction for Sensitivity Encoding with Arbitrary Trajectories. In In Proc. Intl. Soc. Mag. Reson. Med. 9, 2001; p. 767.

29 Liu C, Moseley M. E, and Bammer R. Fast SENSE Reconstruction Using Linear System Transfer Function. In Proc. Intl. Soc. Mag. Reson. Med. 13, 2005; p. 689.

30 Mani M, Jacob M, Guidon A, Magnotta V, and Zhong J. Accelerating non-Cartesian sense for large coil arrays: Application to motion compensation in multishot DWI. In IEEE Int. Symp. Biomed. Imaging (ISBI), 2012. doi: 10.1109/ISBI.2012.6235570.

31 Landman B. A, Bogovic J. A, Wan H, El Zahraa ElShahaby F, Bazin P.-L, and Prince J. L. Resolution of crossing fibers with constrained compressed sensing using diffusion tensor MRI. NeuroImage, 2012, 59(3):2175–86.

32 Wu Y, Zhu Y.-J, Tang Q.-Y, Zou C, Liu W, Dai R.-B, Liu X, Wu E. X, Ying L, and Liang D. Accelerated MR diffusion tensor imaging using distributed compressed sensing. Magn. Reson. Med., 2013. doi: 10.1002/mrm.24721.

33 Bertsekas D. P. Multiplier methods: A survey. Automatica, 1976, 12(2):133–145.

34 Ramani S and Fessler J. A. Parallel MR image reconstruction using augmented Lagrangian methods. IEEE Trans. Med. Imaging., 2011, 30(3):694–706.

35 Yang J and Zhang Y. Alternating Direction Algorithms for l1-Problems in Compressive Sensing. SIAM J. Sci. Comput., 2011, 33(1):250–278.

36 Yang J, Zhang Y, and Yin W. A Fast Alternating Direction Method for TVL1-L2 Signal Reconstruction From Partial Fourier Data. IEEE J. Sel. Top. Signal Process., 2010, 4(2):288–297.

37 Lingala S. G, Hu Y, DiBella E, and Jacob M. Accelerated dynamic MRI exploiting sparsity and low-rank structure: k-t SLR. IEEE Trans. Med. Imaging., 2011, 30(5):1042–54.

38 Tuch D. S. Q-ball imaging. Magn. Reson. Med., 2004, 52(6):1358–72.

39 Daducci A, Canales-Rodríguez E. J, Descoteaux M, Garyfallidis E, Gur Y, Lin Y.-C, Mani M, Merlet S, Paquette M, Ramirez-Manzanares A, Reisert M, Reis Rodrigues P, Sepehrband F, Caruyer E, Choupan J, Deriche R, Jacob M, Menegaz G, Prčkovska V, Rivera M, Wiaux Y, and Thiran J.-P. Quantitative comparison of reconstruction methods for intra-voxel fiber recovery from diffusion MRI. IEEE Trans. Med. Imaging., 2014, 33(2):384–99.

40 Yeh F.-C, Verstynen T. D, Wang Y, Fernández-Miranda J. C, and Tseng W.-Y. I. Deterministic diffusion fiber tracking improved by quantitative anisotropy. PloS one, 2013, 8(11):e80713.

41 Uecker M and Lustig M. Memory-Saving Iterative Reconstruction on Overlapping Blocks of K-Space. In Proc. Intl. Soc. Mag. Reson. Med. 21, 2013; p. 2645.

42 Cauley S. F, Xi Y, Bilgic B, Xia J, Adalsteinsson E, Balakrishnan V, Wald L. L, and Setsompop K. Fast reconstruction for multichannel compressed sensing using a hierarchically semiseparable solver. Magn. Reson. Med., 2014. doi: 10.1002/mrm.25222.

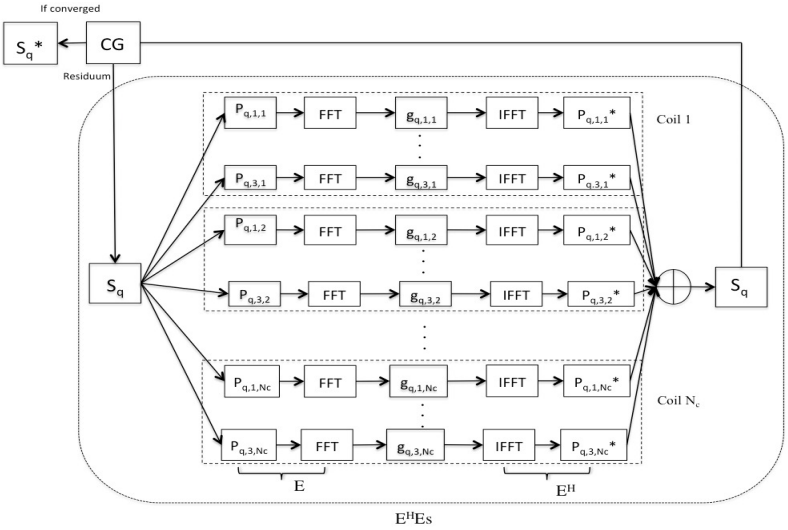

(a) The update of $\mathbf{s}$ using the traditional implementation of $\mathbf{E^H Es}$

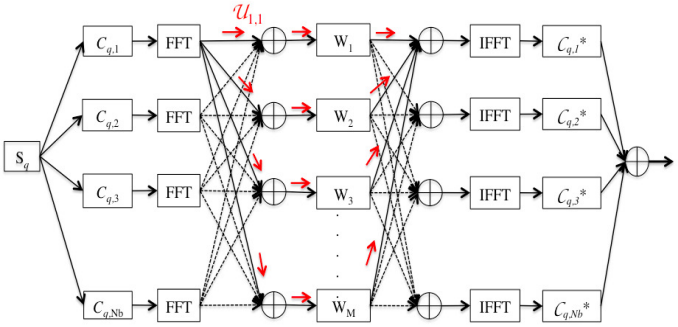

(c) The FFTs get shifted to before the summations and IFFTs shifted to after the summations. All the red arrows indicated together form the weighting $\mathcal{U}_{1,1}$

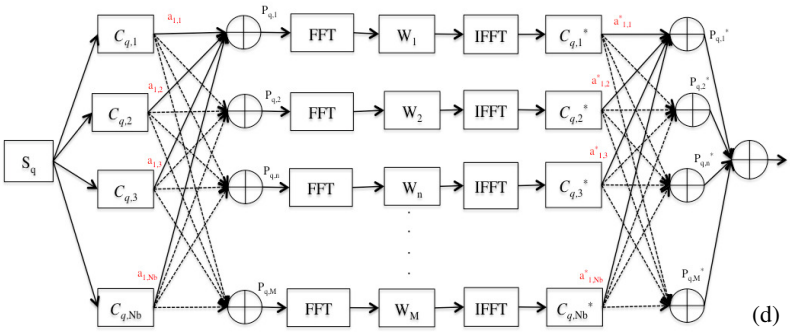

(b) Represent composite sensitivities in terms of the basis functions $\mathbf{C}_j$

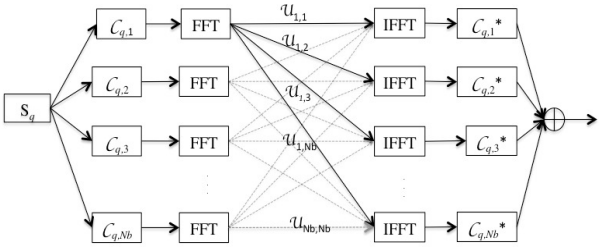

(d) The simplified implementation requires only N_b FFTs and IFFTS

Figure 1: Various implementation of $\mathbf{E^H Es}$ (a) The traditional implementation of $\mathbf{E^H Es}$ in the update of $\mathbf{s}$ is shown. (b) and (c) are the intermediate steps that leads to the final simplified implementation in (d). The various symbols are defined as follows: $\mathbf{S_q}$ is the diffusion weighted image corresponding to the q^{th} diffusion direction, $\mathbf{P}_{q,i,j}$ are the composite sensitivity matrices corresponding to the q^{th} diffusion direction, i^{th} interleaf and j^{th} coil, $\mathbf{g}$ represents the gridding of Cartesian points to non-Cartesian grid followed by gridding back to Cartesian grid and $\mathbf{C}_j$ are the basis functions.

(a) No motion correction	(b) Traditional implementation; t=13.6h	(c) Simplified implementation PCA-based; N_b=36 t=10.22h	(d) Simplified implementation PCA-based; N_b=5 t=1.45h	(e) Difference image (b)−(c)	(f) Difference image (b)−(d)

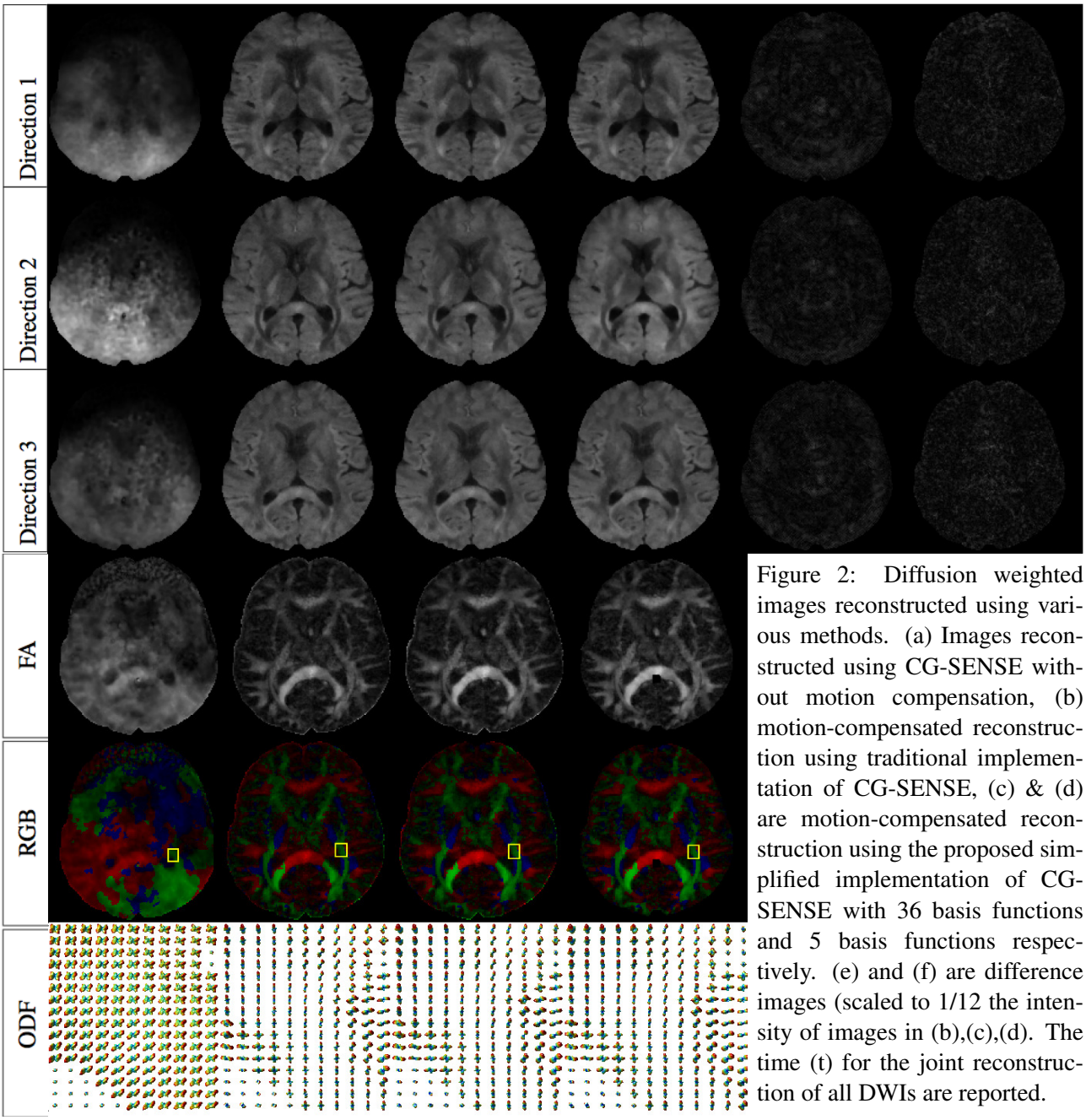

Figure 2: Diffusion weighted images reconstructed using various methods. (a) Images reconstructed using CG-SENSE without motion compensation, (b) motion-compensated reconstruction using traditional implementation of CG-SENSE, (c) & (d) are motion-compensated reconstruction using the proposed simplified implementation of CG-SENSE with 36 basis functions and 5 basis functions respectively. (e) and (f) are difference images (scaled to 1/12 the intensity of images in (b),(c),(d). The time (t) for the joint reconstruction of all DWIs are reported.

Table 1: Scaling of computational complexity with M for the traditional implementation, where M is the the number of composite sensitivities per DWI. Here, the case of a 12-channel acquisition for 64 DWIs is considered.

Number of shots	M per DWI	Memory demands in Megabytes	Time to compute $\mathbf{E^H E s}$ (in sec)
3(R=8)	36	10.125*64=648 Mb	37.11
6(R=4)	72	20.25*64=1.2656 Gb	86.97
11(R=2)	132	37.125*64=2.32 Gb	214.5

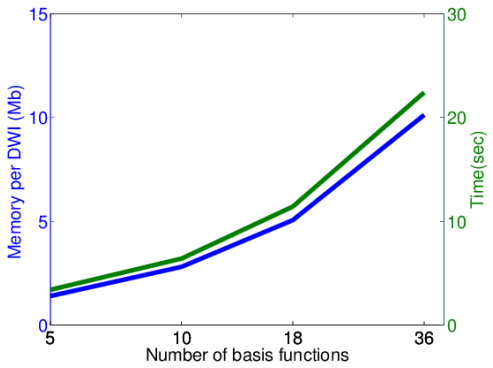

(a) Memory demands and computation time per iteration of $\mathbf{E}^{\mathbf{H}}\mathbf{E}$s for different number of basis functions

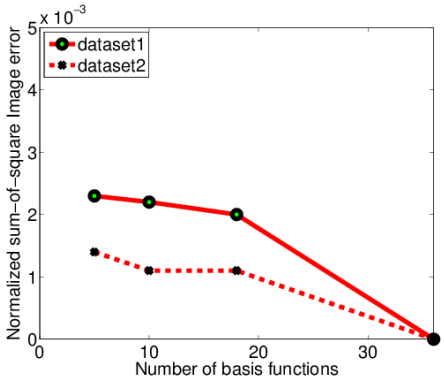

(b) NSSE error for different number of basis functions

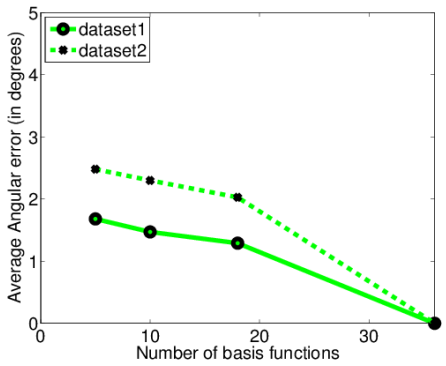

(c) Average odf angular error for different number of basis functions

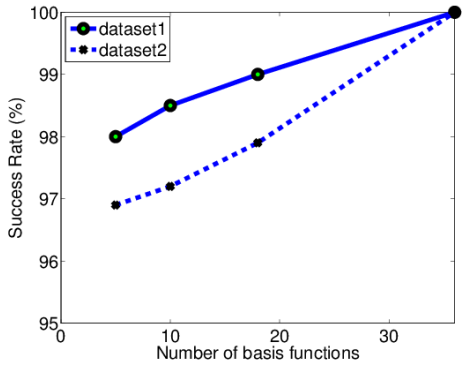

(d) Success rate in finding the correct number of fiber orientations in a voxel for different number of basis functions

Figure 3: The scaling of different parameters with number of basis functions.

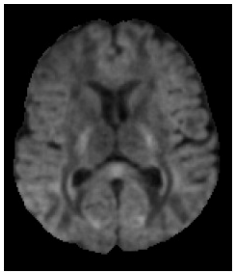

(a) Reference image; time=172.47 sec

Figure 4: Performance comparison between the proposed PCA-based method and the conventional channel compression (SCC). The reference image in (a) is obtained using the traditional implementation of CG-SENSE. The time to reconstruct a single diffusion direction is reported. (Difference images scaled to 1/4th of the dynamic range of reconstructed images.)

PCA-based

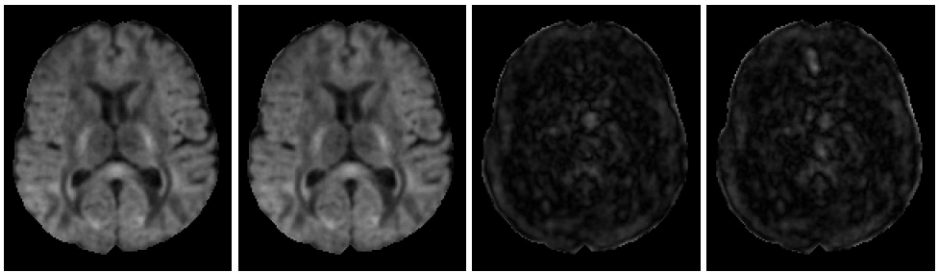

(b) N_b=10; time=4.8 sec

(c) N_b=5; time=2.3 sec

(d) difference image; (a)-(b)

(e) difference image; (a)-(c)

SCC-based

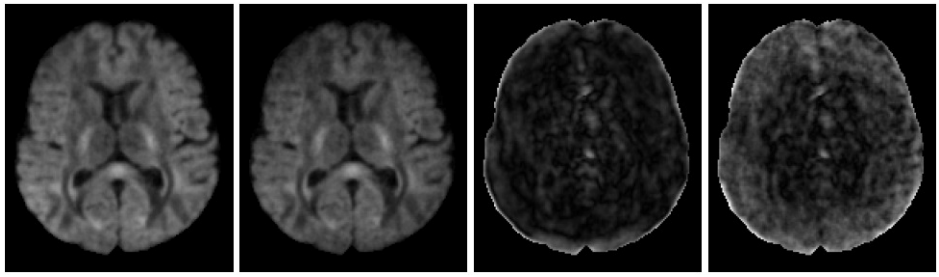

(f) N_{scc}=4; time=34.4 sec

(g) N_{scc}=1; time=8.6 sec

(h) difference image; (a)-(f)

(i) difference image; (a)-(g)